Optical and Quantum Electronics (2025) 57:527
https://doi.org/10.1007/s11082-025-08442-3

A waveguide amplitude modulator based on a graphene plasmonic resonance

Jiří Petráček[1,2] · **Jiří Čtyroký**[3,4] · **Vladimír Kuzmiak**[3]

Received: 22 May 2025 / Accepted: 27 August 2025

Abstract

Photonic waveguides with graphene can enable resonant coupling of the waveguide mode and the graphene plasmonic modes. We demonstrate theoretically that the plasmonic resonance in the hybrid waveguides can be significantly enhanced by employing a graphene nanoribbon with a deep subwavelength width when a lower-order graphene nanoribbon mode and a mode of a bare waveguide are efficiently coupled. A further increase is possible when a single graphene stripe is replaced by a finite array of graphene nanoribbons. This effect may provide a feasible platform for an efficient amplitude modulation which can be employed in the design of specific devices such as low-power modulators, filters, or sensors.

Keywords Photonics · Integrated optics · Graphene · Surface plasmons · Graphene modes · Electro-optic modulation · Coupled mode theory

1 Introduction

Graphene, the iconic representative of two-dimensional materials, exhibits exceptional electrical and optical properties that enable a wide range of nanophotonic applications (Koppens et al. 2011; Grigorenko et al. 2012). Among them, integrated photonic modulators that combine a waveguide with graphene layers have been intensively studied (Sorianello et al. 2020; Koester and Li 2014). Because the surface conductivity of graphene strongly depends on the

✉ Jiří Petráček
petracek@fme.vutbr.cz

[1] Institute of Physical Engineering, Faculty of Mechanical Engineering, Brno University of Technology, Technická 2896/2, Brno 616 69, Czech Republic

[2] Central European Institute of Technology, Brno University of Technology, Purkyňova, 656/123, Brno 612 00, Czech Republic

[3] Institute of Photonics and Electronics, Academy of Sciences of the Czech Republic, v.v.i., Chaberská 57, Prague 8 182 51, Czech Republic

[4] Department of Physical Electronics, Faculty of Nuclear Sciences and Physical Engineering, Czech Technical University in Prague, Břehová 7, Prague 1 115 19, Czech Republic

Published online: 15 September 2025

Fermi level (or chemical potential) E_{F}, which can be tuned by electrical gating, it is possible to modulate the (complex) effective index of modes propagating in such a hybrid waveguide with graphene (Sorianello et al. 2016). Specifically, in the optical and near-infrared (NIR) regions, a graphene layer with $|E_{\mathrm{F}}|$ below the threshold $\hbar\omega/2$ ($\hbar\omega$ being the photon energy) introduces a very strong modal attenuation, while for $|E_{\mathrm{F}}| > \hbar\omega/2$ the attenuation is low, and the real part of the mode index changes with increasing $|E_{\mathrm{F}}|$. Therefore, graphene-based modulators can be utilized for both electro-optic modulation of the amplitude (Liu et al. 2011; Koester and Li 2012) and phase (Mohsin et al. 2015; Sorianello et al. 2018). Modal attenuation can also be controlled optically (Li et al. 2014; Ono et al. 2020).

An intriguing feature of graphene is that it supports surface plasmons (SP), that is, TM polarized surface waves propagating along a graphene sheet (Mikhailov and Ziegler 2007; Hanson 2008; Jablan et al. 2009). Note that graphene can also support TE surface waves (Mikhailov and Ziegler 2007; Hanson 2008); however, these are not considered here. Graphene SPs exhibit extremely high momentum; therefore, their excitation and imaging are challenging problems (Ju et al. 2011; Fei et al. 2011; Chen et al. 2012; Nikitin et al. 2014). Moreover, under usual experimental conditions and assuming the convention $\exp(i\omega t)$ for the time variation, graphene SPs may exist only when the conductivity of graphene σ has the negative imaginary component, $\mathrm{Im}(\sigma) < 0$. In the visible and NIR, the condition corresponds to the region $|E_{\mathrm{F}}| > \hbar\omega/2$, which means that very high levels of $|E_{\mathrm{F}}|$ are required and specialized techniques for lifting $|E_{\mathrm{F}}|$ may be used (Zhang et al. 2014).

Graphene SPs can couple with the waveguide mode provided the graphene layer and the waveguide core are in the close proximity; the phenomenon can be used for enhancing excitation efficiency of graphene SPs (Zhang et al. 2014). We recently theoretically demonstrated that the waveguide phase modulators with graphene can also enable such resonant coupling (Čtyroký et al. 2020b); in this case the waveguide mode evanescently couples with the graphene plasmonic modes (GMs) supported by the finite graphene nanoribbon (Nikitin et al. 2011; Christensen et al. 2012). The graphene resonance occurs when one of the GMs is phase matched with the waveguide mode. Due to the coupling, at the resonance, the mode of the hybrid waveguide with the graphene nanoribbon can experience an attenuation of the order of several dB/mm, which may be employed in design of specific devices such as low-power modulators and sensors. However, the application of the resonant coupling for amplitude modulation in waveguides has not been studied yet. Typically, waveguide modulators with graphene are not based on excitation of graphene plasmons (Liu et al. 2011; Koester and Li 2012; Mohsin et al. 2015; Sorianello et al. 2018). Jang et al. (2018) investigated a planar waveguide modulator that relies on graphene plasmon resonance in plasmonic nanogap; in this case the graphene SPs are excited at the waveguide junction and the resonance occurs in the longitudinal direction. In the geometry studied here, the GMs propagate in the laterally confined structure (nanoribbon) and are excited due to evanescent coupling when the nanoribbon supports the transverse resonance of the phase matched GM. Unlike in previous works dealing with the scattering properties of graphene nanoribbons where the plasmons are excited by an incident electromagnetic wave (Koppens et al. 2011; Ju et al. 2011; Emani et al. 2015), in our structure the graphene plasmons appear due to the coupling with the waveguide mode. Therefore, the aim of this paper is to investigate the resonant coupling in the hybrid waveguides with graphene nanoribbons in more detail and demonstrate that the resonance strength can be significantly enhanced using nanoribbons with a deep subwavelength width. Moreover, we study the effects of the waveguide geometry, the carrier mobility, and the number of nanoribbons on the resonance. The results are obtained with full-wave simulations using COMSOL Multiphysics. However, we also propose a simple theoretical model that provides a physical interpretation of the resonance and explains the enhancement as well as the effects of the other structural parameters. Our findings confirm that the resonant coupling offers an efficient alternative in the design of photonic waveguide modulators.

2 Structure definition and operation principle

We consider a simplified version of graphene-on-silicon modulator inspired by the standard design (Sorianello et al. 2018). The cross-section of the waveguide, shown in Fig. 1, resembles that considered in our previous paper (Čtyroký et al. 2020b) except that a single graphene layer deposited on the top of the rib waveguide is replaced by a finite set of graphene nanoribbons that are parallel with the waveguide axis and placed symmetrically with respect to the *yz* plane. The structural parameters, which are defined in Table 1, are chosen in accord with the operating wavelength of $\lambda = 6\ \mu$m. The refractive indexes of Si and SiO_2 are taken from Shkondin et al. (2017) and Kischkat et al. (2012), respectively. We did not perform any optimization of the waveguide geometry, instead we will discuss the effect of the geometrical parameters on the modulation performance.

The optical properties of graphene are determined by its complex surface conductivity σ, which can be calculated within various approximations, see, e.g., Hanson (2008); Koppens et al. (2011). Here we used the closed formula provided by Chang et al. (2014). The conductivity σ depends on the frequency ω, the Fermi level E_F, the intraband scattering rate γ (or the relaxation time $\tau = \gamma^{-1}$) and temperature *T*, which we set $T = 300$ K. The relaxation time is an important parameter that affects the SP propagation distance (Jablan et al. 2009) and it is related to the graphene quality. τ can be estimated from the dc mobility μ using the formula (Jablan et al. 2009; Koppens et al. 2011)

$$\tau = \frac{\mu E_\mathrm{F}}{e v_\mathrm{F}^2}, \tag{1}$$

where e is the elementary charge and $v_\mathrm{F} \approx 10^6$ m/s is the Fermi velocity. Unless otherwise stated, in the following calculations we set $\tau = 0.2$ ps, which corresponds with $\mu = 4000\ \mathrm{cm^2\,V^{-1}\,s^{-1}}$ at $E_\mathrm{F} = 0.5$ eV. This choice represents a moderate value of μ, consis-

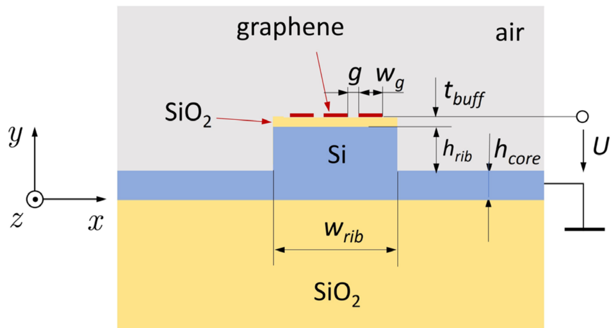

Fig. 1 The hybrid rib waveguide with graphene nanoribbons

Table 1 Structural parameters

Symbol	Value	Description
λ	6.000 μm	Operating wavelength (in vacuum)
w_{rib}	2.800 μm; except Fig. 4a, c	Rib width
h_{rib}	0.900 μm; except Fig. 4b, c	Rib elevation
h_{core}	0.500 μm; except Fig. 4b, c	Core height
t_{buff}	20 nm; except Fig. 4a, c	SiO_2 buffer thickness
w_{g}	Varied	Graphene nanoribbon width
n_{ribbons}	Varied	Number of graphene nanoribbons
g	Varied	Gap between graphene nanoribbons
$n(\text{SiO}_2)$	$1.2713 - 0.0016067i$	SiO_2 refractive index
$n(\text{Si})$	$3.4698 - 0.0000017002i$	Si refractive index
E_{F}	Varied	Fermi level
σ	Determined by E_{F}	Graphene surface conductivity
$N_{\text{eff},0}$	$2.97498 - 0.0000335i$; except Fig. 4	Effective mode index of the waveguide without graphene

tent with the literature (Fei et al. 2011; Koester and Li 2012; Sorianello et al. 2020). However, other loss mechanisms, such as effect of optical phonons or many-body interactions, that are not described with Eq. (1) may influence the relaxation time too. Therefore, our definition of τ as a constant serves for demonstration purposes and it is appropriate when the investigated graphene resonance occurs near the same value of E_{F} and/or when τ is limited by the other loss mechanisms.

In the COMSOL simulations, we represented graphene stripes by a boundary condition involving σ; details of the whole procedure are described in Čtyroký et al. (2020a, 2020b).

The coupling is a generic effect, so the unusual choice of the mid-infrared range is only of technical convenience, and it is primarily motivated to achieve deep subwavelength width of the nanoribbons. An additional advantage of the selected range is that it allows amplitude modulation with realistic values of the Fermi level, $|E_{\text{F}}| \sim 0.5$ eV, as opposed to the visible and NIR, where extremely high values of $|E_{\text{F}}|$ larger than ~ 1.5 eV would be required.

For the given geometry, the efficient modulation can be achieved with quasi-TE modes only as the coupling is due to the components of the electric field that are parallel with graphene layers (Čtyroký et al. 2020b). Therefore, we performed a set of numerical experiments and calculated the effective mode index N_{eff} of the quasi-TE mode of the hybrid waveguide for various structural parameters.

We first consider the hybrid waveguide with a single graphene layer ($n_{\text{ribbons}} = 1$). The behavior of the effective mode index N_{eff} as a function of the Fermi level E_{F} is shown in Fig. 2a and b for two different widths of the graphene stripe w_{g}. For the wide stripe, $w_{\text{g}} = 2000$ nm, the structure exhibits typical features of the integrated graphene modulators. The real component of the variance ΔN_{eff} of the effective index due to a graphene layer decreases almost monotonically with increasing E_{F} provided $E_{\text{F}} > \hbar\omega/2 \approx 0.1$ eV (Fig. 2a) while modal loss, $b = -20\log_{10}(e)\, k_0\, \text{Im}(N_{\text{eff}})$, $k_0 = 2\pi/\lambda$, becomes signifi-

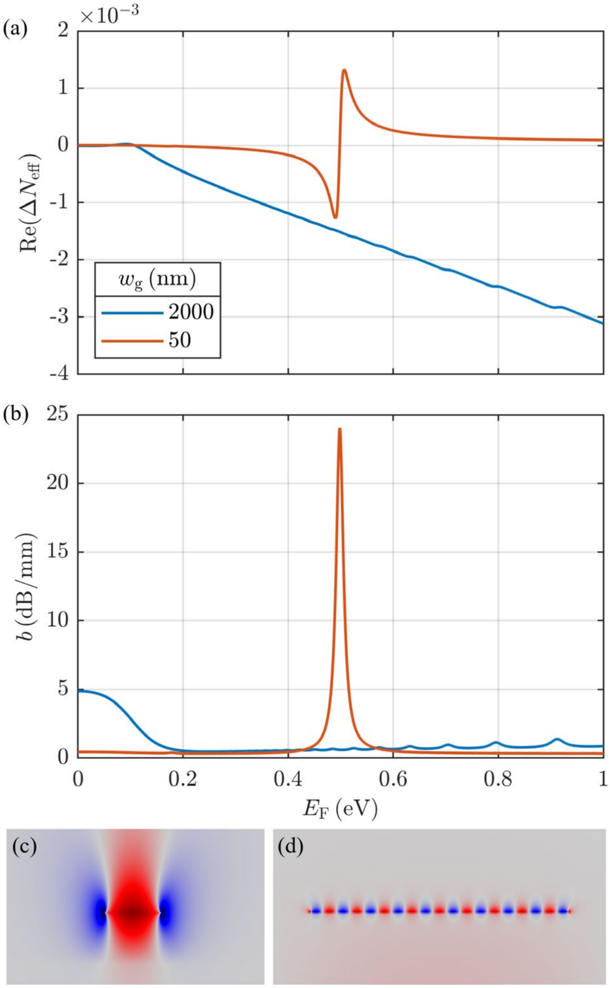

Fig. 2 **a**, **b** Modal spectra for the waveguide with a single graphene stripe ($n_{\mathrm{ribbons}} = 1$) for two different values of the graphene stripe width w_{g}. **a** The real component of the change of the effective mode index $\Delta N_{\mathrm{eff}} = N_{\mathrm{eff}} - N_{\mathrm{eff},0}$, where N_{eff} and $N_{\mathrm{eff},0}$ are the effective indexes of the waveguide with graphene and the bare Si waveguide, respectively, and **b** modal loss b vs. the Fermi level E_{F}. **c**, **d** The dominant component of the electric field E_x near the graphene ribbon at the resonance; **c** $w_{\mathrm{g}} = 50$ nm, $E_{\mathrm{F}} = 0.49825$ eV, **d** $w_{\mathrm{g}} = 2000$ nm, $E_{\mathrm{F}} = 0.91225$ eV

cant when $E_{\mathrm{F}} < \hbar\omega/2$ (Fig. 2b). The dependencies can be explained by considering the graphene stripe as a perturbation of the waveguide without graphene. The variance ΔN_{eff} depends on the overlap of the unperturbed mode of the bare waveguide and the conductivity distribution in the graphene stripe (Ralevič et al. 2014; Čtyroký et al. 2020a). Indeed, the overlap becomes negligible for narrow stripes and therefore the described behavior disappears when $w_{\mathrm{g}} = 50$ nm. Instead, we observe a strong resonance due to the coupling of the unperturbed waveguide mode with a suitable GM; in particular, with the second-order GM [the mode is labeled with 2 in Nikitin et al. (2011)] when $w_{\mathrm{g}} = 50$ nm. Figure 2c displays modal field near the nanoribbon at the resonance. One can see that the field exhibits a profile typical for the second-order GM, which proves its excitation. Note, that the coupling with the first-order GM [the fundamental "edge" GM in Nikitin et al. (2011)] cannot occur due to different parity as well as due to large effective index mismatch.

The effect can be interpreted in terms of a simple approximate model, which is based on the coupled mode theory and described in more detail in Appendix A. The model confirms our conjecture that the resonance occurs as a consequence of the coupling between a low loss mode of dielectric waveguide (indicated by the subscript 1) and a plasmonic mode (indicated by the subscript 2) that exhibits a strong loss. Equation (A8), with the substitution $\Delta\beta_1 = k_0\Delta N_{\text{eff}}$, approximately describes the Lorentzian shape of the resonance shown in Fig. 2a and b for $w_{\text{g}} = 50$ nm, as one can infer from Fig. 8. The model also predicts [see Eq. (A9)] that, at the resonance, $\text{Re}(\Delta N_{\text{eff}}) \approx 0$ and

$$\text{Im}(\Delta N_{\text{eff}}) \approx \frac{\kappa^2}{k_0\beta_2''}, \tag{2}$$

where the parameter κ, defined in Eqs. (A7) and (A4), describes the coupling and β_2'' is the imaginary component of the propagation constant of the excited GM.

A very weak resonant coupling occurs also for the waveguide with the wide stripe, $w_{\text{g}} = 2000$ nm, as indicated by the small ripples in Figs. 2a and b. The modal profile in Fig. 2d, corresponding to one of the resonances, reveals excitation of a higher-order GM. Note that the wide stripe supports only resonances with higher-order GMs in the given range of E_{F}; this is consistent with the fact that resonances of the individual GMs move towards higher values of E_{F} with increasing w_{g}. Clearly, the resonance strength (i.e., modal loss *b* at the resonance) decreases with increasing w_{g} or with increasing order of a particular GM that sets into the resonance. This behavior, demonstrated in Fig. 3, can be qualitatively explained in terms of Eq. (2) as follows.

The value of the propagation constant β_2 of the applicable GM is given by the resonance condition. Therefore, the resonance strength depends on $\kappa^2 = K_{12}K_{21}$. The perturbation term $(\varepsilon - \varepsilon_1)$ in the definition of the coupling coefficient K_{12} [see Eq. (A4)] is nonzero only in the graphene stripe, which is described by the surface conductivity σ. Therefore, by using similar arguments as in Čtyroký et al. (2020a), one can write

$$K_{12} = -ic\mu_0\sigma \int_{-w_{\text{g}}/2}^{w_{\text{g}}/2} \mathcal{E}_{1x}\mathcal{E}_{2x}\, dx, \tag{3}$$

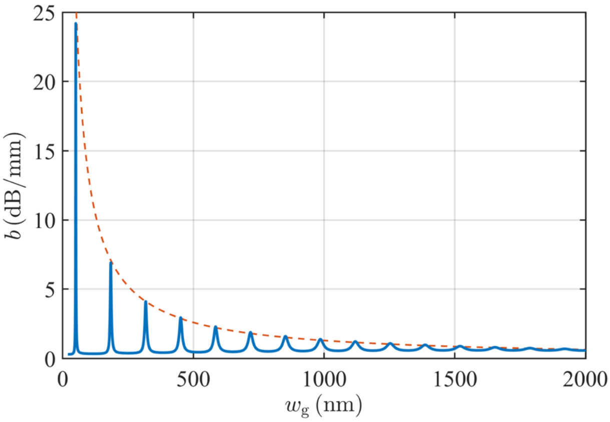

Fig. 3 Modal loss *b* vs. width of the graphene stripe w_{g} (the solid line). Other parameters: $E_{\text{F}} = 0.5$ eV, $n_{\text{ribbons}} = 1$. The order of the GM excited at the resonance increases with increasing w_{g}. The dashed line indicates the dependence $b = C/w_{\text{g}}$, where *C* was determined by fitting the peaks

where $\mathcal{E}_{1x}$ and $\mathcal{E}_{2x}$ describe the electric field distributions of the interacting modes, i.e., the mode of the bare waveguide and GM, respectively, we neglect minor $\mathcal{E}_z$ components of the modal fields, and we integrate over the width of the graphene stripe at y corresponding with the stripe position. To estimate the behavior of the integral we neglect the weak dependence of $\mathcal{E}_{1x}$ on x and assume that GMs may be approximately viewed as guided waves resulting from interference between two graphene SPs that propagate under some (complex) angle with respect to the nanoribbon axis and reflect from its edges (Čtyroký et al. 2020b). Accordingly, the GMs with an appropriate symmetry for the coupling exhibit standing-wave patterns (similar to the ones displayed in Fig. 2c and d) as

$$\mathcal{E}_{2x} \approx \frac{A(k_{2x})}{\sqrt{w_\mathrm{g}}} \cos(k_{2x}x). \tag{4}$$

The form of the amplitude $A/\sqrt{w_\mathrm{g}}$, where A depends on the transverse wave vector k_{2x}, is obtained from the normalization procedure for GMs, see Eq. (A5). At arbitrary resonance, k_{2x} acquires (approximately) the same value determined by β_2 (Čtyroký et al. 2020b), in other words, the resonant value of k_{2x} is independent of w_g or of the order of GM. We see that the magnitude of K_{12} at the resonance scales as $1/\sqrt{w_\mathrm{g}}$. By using similar arguments, namely that $\mathcal{E}_{2x}$ contributes to the integral in K_{21} only in the range $-w_\mathrm{g}/2 < x < w_\mathrm{g}/2$, it is possible to estimate, that the magnitude of K_{21} at the resonance exhibits the same dependence on w_g as K_{21}. We conclude that κ^2 at the resonance as well as the resonance strength scales as $1/w_\mathrm{g}$. This trend is indicated in Fig. 3, where we observe reasonable agreement with rigorous simulations.

For wide graphene stripes, $\kappa^2 \to 0$ and the resonant coupling can be neglected. On the other hand, the resonance can be significantly enhanced when graphene nanoribbons with a deep subwavelength width are considered, as it is shown in Fig. 3. This is the main result of this work. The order of the excited GM decreases simultaneously with decreasing w_g, therefore the strongest resonance occurs for the second-order GM when $w_\mathrm{g} = 50.2$ nm. The value of the observed loss ~ 25 dB/mm suggests that the design presented here may provide a feasible platform for an efficient amplitude modulation.

In the following analysis, we focus on the systems that support the coupling with the second-order GM. To keep a reasonable value of E_F, we fix the nanoribbon width at $w_\mathrm{g} = 50$ nm.

3 Effects of waveguide geometry, carrier mobility, and number of nanoribbons

The resonant coupling can be influenced by the geometry of the bare waveguide. To evaluate the effect we calculated the dependencies of N_eff on E_F in a wider range of the geometrical parameters and, in Fig. 4, we display loss at the resonance, i.e., maximums of the $b(E_\mathrm{F})$ curves. The observed trends can be understood by realizing that the coupling coefficients K_{12} and K_{21} depend on the modal overlaps; namely, that $|K_{12}|$ scales with the magnitude of the normalized field distribution $\mathcal{E}_{1x}$ at the nanoribbon position, see Eq. (3).

Figure 4a demonstrates that for smaller values of the rib width w_rib, approximately for $w_\mathrm{rib} < 2.2\,\mu$m, the resonant loss increases with w_rib. This is because the confinement of

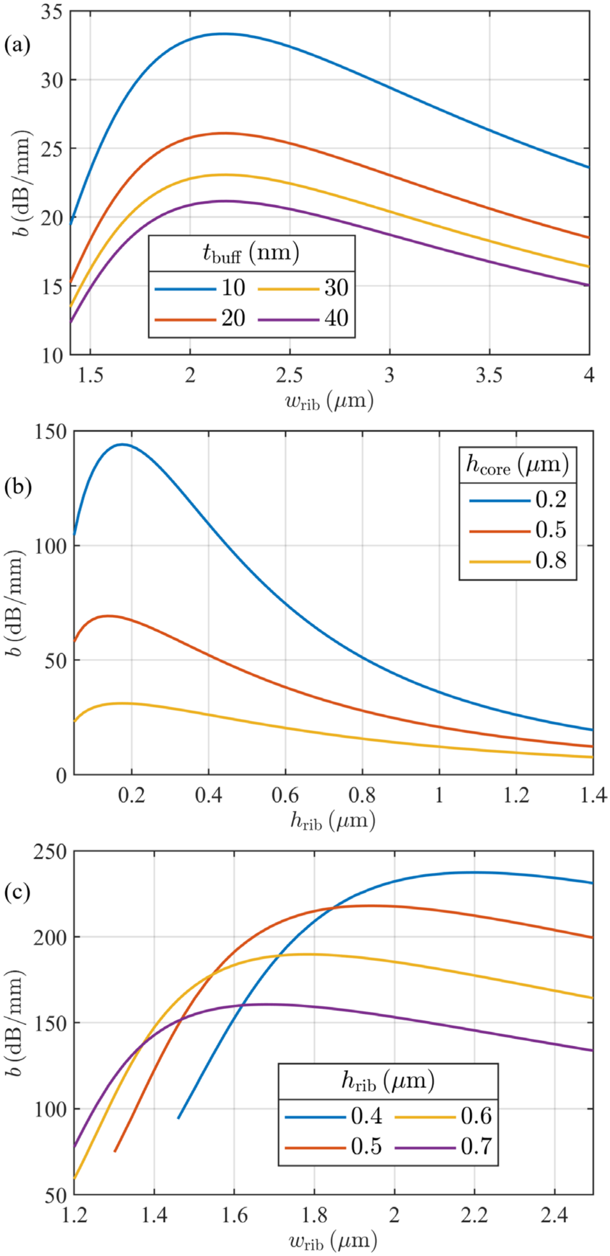

Fig. 4 The effect of the waveguide geometry on the resonance curve. **a** Loss b at the resonance vs. **a** the rib width w_{rib} for various values of the buffer thickness t_{buff}; **b** the rib elevation h_{rib} for various values of the core height h_{core}; and **c** w_{rib} for $h_{\mathrm{core}} = 0$, $t_{\mathrm{buff}} = 10\,\mathrm{nm}$, and various values of h_{rib}. Other parameters: $w_{\mathrm{g}} = 50\,\mathrm{nm}$, $n_{\mathrm{ribbons}} = 1$

the waveguide mode in the Si core increases with w_{rib} leading to better localization of $\mathcal{E}_{1x}$ in the lateral (x) direction near $x = 0$ in the considered range of w_{rib} and, therefore, to the increasing magnitude of $\mathcal{E}_{1x}$. However, for $w_{\mathrm{rib}} > 2.2\,\mu\mathrm{m}$, the increase in the modal confinement with w_{rib} almost saturates, while the cross-sectional area of the Si core still increases, resulting in decreasing the magnitude of $\mathcal{E}_{1x}$. Consequently, in this regime the resonant loss decreases with w_{rib}. Figure 4a also illustrates the effect of the buffer thickness $t_{\rm buff}$. Indeed, decreasing $t_{\rm buff}$ enhances the resonant loss, due to better overlap of the interacting modes.

In Fig. 4b, we observe that the resonant loss decreases with increasing $h_{\rm rib}$, provided $h_{\rm rib}$ is above a certain threshold value $\sim 0.15\,\mu$m, and as well as with increasing $h_{\rm core}$. Both the trends correspond to the fact that the Si core area increases with either of these two parameters leading to decreasing the magnitude of $\mathcal{E}_{1x}$. When $h_{\rm rib}$ is below the threshold, the resonant loss increases with $h_{\rm rib}$ due to increasing localization of the waveguide mode in the vertical (*y*) direction near the nanoribbon position. The simulations also revealed the fact that the position of the Fermi level $E_{\rm F}$ at the resonance is almost constant when $t_{\rm buff}$ is fixed. This is because the parameters $w_{\rm rib}$, $h_{\rm rib}$, and $h_{\rm core}$ do not have any realistic impact on the effective index of the second-order GM. On the contrary, the presence of the Si core can somewhat modify the effective index of GMs; the change increases with decreasing $t_{\rm buff}$. Therefore, $E_{\rm F}$ at the resonance slightly increases with decreasing $t_{\rm buff}$; for the values of $t_{\rm buff}$ specified in Fig. 4a (in ascending order) the resonance occurs at 0.59 eV, 0.50 eV, 0.47 eV, and 0.46 eV, respectively. The trends observed in Fig. 4a and b indicate that the best performance should be obtained with minimal values of $h_{\rm core}$ and $t_{\rm buff}$. Therefore, in Fig. 4c, we investigate structures with $h_{\rm core} = 0$ and $t_{\rm buff} = 10\,$nm. Indeed, the resonance in such rectangular waveguide is significantly enhanced; the resonant loss can reach almost 240 dB/mm when $h_{\rm rib} = 0.4\,\mu$m. We also observe that the maximum of the resonant loss increases with decreasing $h_{\rm rib}$ and its position shifts towards bigger values of $w_{\rm rib}$. However, these results should be taken with caution as decreasing $h_{\rm rib}$ drives the mode towards its cut-off (see the curves for $h_{\rm rib} = 0.4\,\mu$m and $h_{\rm rib} = 0.5\,\mu$m, which exhibit the cut-off in the displayed range of $w_{\rm rib}$). Consequently, the mode in the structures with parameters of Fig. 4c is only weakly guided, which is not desirable for practical applications. Similarly, the mode of the rib waveguides, such as studied in Fig. 4a and b, approaches the cut-off with decreasing $h_{\rm rib}$. Therefore, any further structural optimization should take into account the effect of the modal confinement, and, in the following analysis, we return to the initial geometrical parameters quoted in Tab. 1. The modulator performance can also be affected by the relaxation time τ. To address the problem we determined τ by using Eq. (1) and considered graphene with the mobility μ in a realistic range $500\,{\rm cm}^2\,{\rm V}^{-1}\,{\rm s}^{-1} < \mu < 10^4\,{\rm cm}^2\,{\rm V}^{-1}\,{\rm s}^{-1}$, which corresponds with $0.025\,{\rm ps} < \tau < 0.5$ ps at $E_{\rm F} = 0.5$ eV. The calculated dependencies of $N_{\rm eff}$ on $E_{\rm F}$ always exhibit the resonant behavior, such as that observed in Fig. 2a and b for $w_{\rm g} = 50\,$nm. The position of the resonance, $E_{\rm F} \doteq 0.5$ eV, does not change appreciably with μ; this is consistent with the fact that μ affects mainly the loss, therefore it has only a minor influence on ${\rm Re}(N_{\rm eff})$, which determines the resonance position. However, as shown in Fig. 5, the parameters that are related to the loss can vary significantly. We observe that the loss b at the resonance scales with μ, approaching the value 52 dB/mm when a high quality graphene with $\mu = 10^4{\rm cm}^2\,{\rm V}^{-1}\,{\rm s}^{-1}$ is used. In the same limit, FWHM of the $b(E_{\rm F})$ curve can be as narrow as 0.0076 eV, suggesting that very small change of $E_{\rm F}$ is necessary for the amplitude modulation. On the other hand, the modulation is significantly deteriorated when a low quality graphene is used, namely for $\mu < 1500\,{\rm cm}^2\,{\rm V}^{-1}\,{\rm s}^{-1}$. Note, that during the calculation we also confirmed that the resonance curve obtained for $\mu = 4000\,{\rm cm}^2\,{\rm V}^{-1}\,{\rm s}^{-1}$ is almost identical with the curve obtained for $\tau = 0.2$ ps. This justifies our conjecture about the constant value of the relaxation time τ used in the other calculations.

Next, in order to examine further possible enhancement of the devices with $\tau = 0.2\,$ps, we consider the structure which contains a periodic arrangement of $n_{\rm ribbons}$ graphene nanorib-

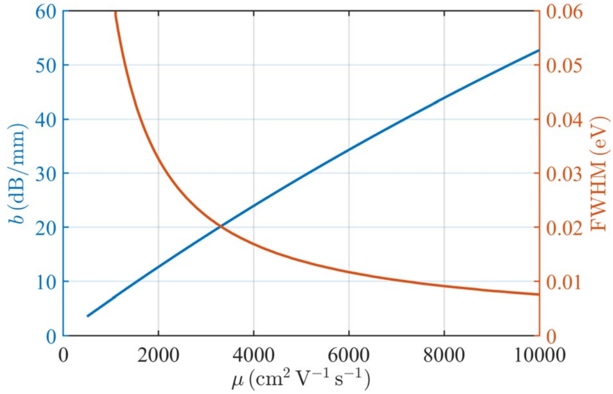

Fig. 5 The effect of the carrier mobility μ on the resonance curve. Loss b at the resonance and FWHM vs. μ for a single nanoribbon with the width $w_\mathrm{g} = 50\,\mathrm{nm}$. The relaxation time τ was calculated by using Eq. (1)

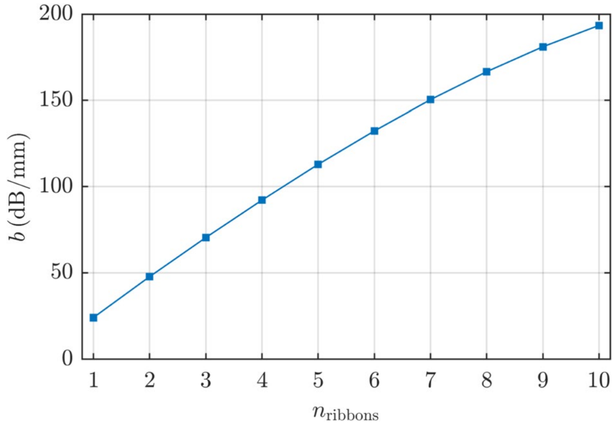

Fig. 6 The effect of the nanoribbon number n_ribbons. Loss b at the resonance vs. n_ribbons. Other parameters: $w_\mathrm{g} = 50\,\mathrm{nm}$, $g = 100\,\mathrm{nm}$

bons. In Fig. 6 we show the predicted behavior for the loss b at the resonance obtained from numerical simulations. One can see that b scales almost linearly with n_ribbons, in particular for smaller values of n_ribbons when all the nanoribbons are close to the center of the rib waveguide. This agrees with our model. Consider, for example, calculation of the overall coupling coefficient K_{12} through Eq. (3), where we now integrate over all the nanoribbons. For smaller values of n_ribbons, $\mathcal{E}_{1x}$ is approximately constant. However, we also have to change the normalization constant in Eq. (4), therefore the integral scales as $\sqrt{n_\mathrm{ribbons}}$. K_{21} exhibits the identical behavior. As a result κ^2 is nearly linearly proportional to n_ribbons. Indeed, the value of E_F at the resonance slightly increases with increasing n_ribbons (not shown in Fig. 6); however, for the specific parameters we always obtained $E_\mathrm{F} \approx 0.5$ eV.

Finally, we examine the effect of the gap g between the adjacent graphene nanoribbons on the plasmonic resonance, see Fig. 7. The dependence of the Fermi level E_F on g reveals that for wider gaps, when approximately $g > 150\,\mathrm{nm}$, the GMs excited in the individual nanoribbons do not mutually interact as the resonant position of E_F remains constant. In this regime, the resonant loss b decreases with increasing g due to increasing distance of the lateral nanoribbons from the center. Again, this agrees with our model. $|\mathcal{E}_{1x}|$ decreases with increasing $|x|$, thus the product $K_{12}K_{21}$ is reduced when g increases and w_g is fixed. On the other hand, when g decreases, namely for $g < 50\,\mathrm{nm}$, GMs in the adjacent nanoribbons

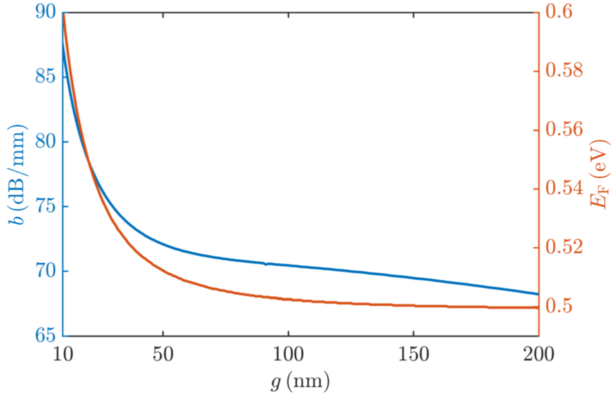

Fig. 7 The effect of the gap width g. Loss b and the Fermi level E_F at the resonance vs. g. Other parameters: $w_g = 50$ nm, $n_{\text{ribbons}} = 3$

couple, resulting in the shift of the resonance towards higher E_F. The shift is accompanied with the increase of the resonant loss b. Note that singular-like behavior of g and E_F in the limit of vanishing g indicates a failure of the model of the graphene due to absence of the non-local parameters rather than a realistic effect.

4 Conclusion

In summary, we examined theoretically the resonant coupling between the waveguide mode and graphene plasmonic modes propagating along a graphene nanoribbon. We have found that the strength of the resonance can be significantly enhanced using a nanoribbon with a deep subwavelength width. The order of the graphene mode excited at the resonance decreases with decreasing nanoribbon width, therefore the strongest resonance occurs for the second-order graphene mode, which is the lowest order graphene mode that can couple with the waveguide mode. A further increase of the plasmonic resonance by order of magnitude is possible when using a finite array of graphene nanoribbons instead of the single one.

It is important to note that the parameters of the resonance (the loss at the resonance and FWHM) are strongly influenced by the relaxation time τ (or the mobility μ) of the graphene nanoribbons. For the selected geometry, an efficient amplitude modulation with the extinction ratio (= the loss at the resonance − the loss when the Fermi level E_F is shifted by FWHM from the resonance) $>$ 20 dB/mm and FWHM $<$ 0.08 eV requires $\mu > 4000$ cm^2 V^{-1} s^{-1}, i.e., $\tau > 0.2$ ps at $E_F = 0.5$ eV. We also analyzed dependence of the resonant coupling on the geometrical parameters of the bare waveguide. The findings indicate that by varying the waveguide geometry it is possible to achieve a significant enhancement of the resonance parameters; however, one has to choose a trade-off values that are from the point of view of the modulation performance suitable for realistic applications.

The results were obtained with rigorous full-wave simulations. However, we also employed the coupled mode theory and developed a simple qualitative model that provides a physical interpretation of the observed behavior. The model confirms that the resonance occurs as a consequence of the coupling between a low loss mode of dielectric waveguide and a plasmonic mode that exhibits a strong loss. The model also provides an explicit description of the resonance shape, and explains the enhancement.

We note that the harnessing of the resonant coupling between a bare waveguide mode and a lower-order graphene mode has not been considered as yet. Our findings confirm that the resonant coupling offers an efficient alternative in design of photonic waveguide modulators provided that devices with high quality graphene nanoribbons are available. The effect may find application in schemes for an efficient excitation of graphene plasmonic modes as well as for an enhanced amplitude modulation. The latter can be employed in design of specific devices such as low-power modulators, frequency filters, modal filters or sensors.

Appendix A: Coupled mode description of the resonant coupling

Coupling of a mode of a bare silicon waveguide with plasmonic modes of a graphene nanoribbon on top of the silicon waveguide can be considered as a mutual coupling among modes of parallel waveguides.

In the Appendix we employ principles of the coupled mode theory (Kogelnik 1975; Haus et al. 1987) to obtain general formulation not limited to the geometries studied in the paper. Then we derive a simple approximate expression that describes the resonant coupling between two modes in the regime when one of the modes exhibits a strong loss.

The whole structure is defined with the relative permittivity distribution $\varepsilon(x, y, z)$. We assume that the total field in the structure can be expanded in terms of modes of simpler, z-invariant, structures ('waveguides'). We prescribe the permittivity $\varepsilon_m(x, y), m = 1, 2, \ldots,$ to each individual mode m. Generally, we assume that the quantities ε and ε_m are complex tensors. Therefore, the formulation is obtained with the approach applicable to the systems with a complex permittivity profile such as that used in Ye et al. (2010).

The m-th mode is described with the transverse electric and magnetic field distribution $\vec{\mathcal{E}}_m$ and $\vec{\mathcal{H}}_m$, respectively, and the corresponding propagation constant β_m. The modal expansion reads

$$\vec{E}\left(x,y,z\right)=\sum_{m}A_m\left(z\right)\vec{\mathcal{E}}_m\left(x,y\right),\quad \vec{H}\left(x,y,z\right)=\sum_{m}A_m\left(z\right)\vec{\mathcal{H}}_m\left(x,y\right), \tag{A1}$$

The expansion coefficients A_m are obtained by solving the system

$$i\sum_{n}O_{mn}\frac{dA_n}{dz}=\sum_{n}\left(O_{mn}\beta_m+K_{mn}\right)A_n, \tag{A2}$$

where

$$O_{mn}=c\mu_0\iint\left(\vec{\mathcal{E}}_m\times\vec{\mathcal{H}}_n+\vec{\mathcal{E}}_n\times\vec{\mathcal{H}}_m\right)\cdot\hat{z}\,dxdy, \tag{A3}$$

$$K_{mn}=k_0\iint\vec{\mathcal{E}}_m^{-}\cdot\left(\varepsilon-\varepsilon_m\right)\vec{\mathcal{E}}_n\,dxdy, \tag{A4}$$

c is the velocity of light, μ_0 is the vacuum permeability, k_0 is the vacuum wavenumber, $\vec{\mathcal{E}}_m^{-}$ denotes the electric field distribution of the mode with inverted $\mathcal{E}_z$ component, and we integrate over the cross-section of the whole waveguide structure. From now on, we will also require that the modes are normalized as

$$O_{mm} = 1. \tag{A5}$$

Now we apply the general formalism to the systems where ε does not depend on z and search for the supermodes. Because we are interested in a simple approximate description of the coupling between two modes (e.g., a waveguide mode and a graphene mode) we use only these two modes in the modal expansion, i.e., we have $m, n = 1, 2$ in Eqs. (A1)–(A5). Furthermore, in Eq. (A2), we neglect the terms $O_{12} = O_{21}$ as $|O_{12}| = |O_{21}| \ll 1$ and similarly we neglect K_{11} and K_{22} with respect to β_1 and β_2, respectively.

The supermodes are the solutions of Eq. (A2) of the form $A_m(z) = A_m(0)\exp(-i\gamma z)$. It is straightforward to show that, within the described approximations, the propagation constants of the supermodes are given by the relation

$$\gamma_{1,2} = \bar{\beta} \pm \sqrt{\delta^2 - \kappa^2}, \tag{A6}$$

where

$$\bar{\beta} = \frac{\beta_1 + \beta_2}{2}, \quad \delta = \frac{\beta_1 - \beta_2}{2}, \quad \kappa^2 = K_{12}K_{21}. \tag{A7}$$

Finally, we consider the regime when one of the individual modes is (at least approximately) lossless, $\beta_1 \in \mathbb{R}$, while the other one with $\beta_2 = \beta_2' + i\beta_2''$ ($\beta_2', \beta_2'' \in \mathbb{R}$), exhibits a strong loss, such that $|\delta|^2 \gg |\kappa|^2$ in Eq. (A6). This allows us to estimate the variation $\Delta\beta_1 = \gamma_1 - \beta_1$ of the propagation constant of the lossless mode due to the coupling as

$$\Delta\beta_1 \approx \frac{\kappa^2}{\beta_1 - \beta_2' - i\beta_2''}. \tag{A8}$$

Fig. 8 The change of the propagation constant $\Delta\beta_1$ as a function of the detuning $\beta_1 - \beta_2''$. For the calculation we used Eq. (A8) and assumed that $\kappa^2 \in \mathbb{R}$

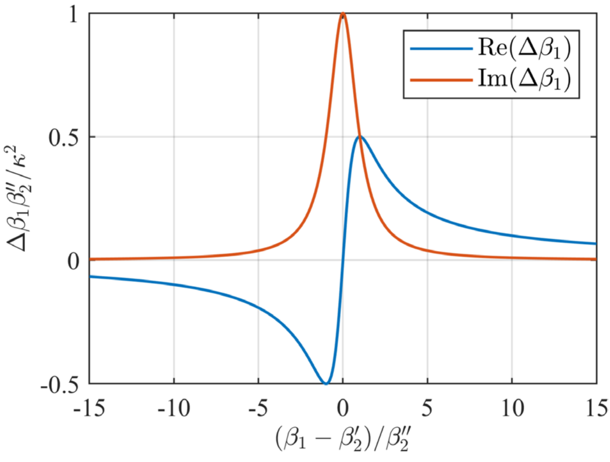

One can see that $\Delta\beta_1$ exhibits a resonant behavior with a Lorentzian profile demonstrated in Fig. 8. At the resonance $\beta_1 = \beta_2'$, and Eq. (A8) reduces to

$$\Delta\beta_1 \approx i\frac{\kappa^2}{\beta_2''}. \tag{A9}$$

Acknowledgements The authors gratefully acknowledge the support of the Ministry of Education, Youth, and Sports of the Czech Republic (grant no. 8J24FR002).

Author contributions Conceptualization: JP; Investigation: JP, JČ, VK; Methodology: JP, JČ, VK; Visualization: JP; Writing—original draft: JP, VK; Writing—review & editing: JČ, VK. All authors read and approved the final manuscript.

Funding Open access publishing supported by the institutions participating in the CzechELib Transformative Agreement. This work was supported by the Ministry of Education, Youth, and Sports of the Czech Republic (grant number 8J24FR002).

Data availability No datasets were generated or analysed during the current study.

Declarations

Conflict of interest The authors declare no Conflict of interest.

Ethical approval Not applicable.

References

Chang, Y.C., Liu, C.H., Liu, C.H., Zhong, Z., Norris, T.B.: Extracting the complex optical conductivity of mono- and bilayer graphene by ellipsometry. Appl. Phys. Lett. **104**, 261909 (2014)

Chen, J., Badioli, M., Alonso-González, P., et al.: Optical nano-imaging of gate-tunable graphene plasmons. Nature **487**, 77–81 (2012)

Christensen, J., Manjavacas, A., Thongrattanasiri, S., Koppens, F.H.L., García De Abajo, F.J.: Graphene plasmon waveguiding and hybridization in individual and paired nanoribbons. ACS Nano **6**(1), 431–440 (2012)

Čtyroký, J., Petráček, J., Kwiecien, P., Richter, I., Kuzmiak, V.: Graphene on an optical waveguide: comparison of simulation approaches. Optical and Quantum Electronics **52**, 149 (2020)

Čtyroký, J., Petráček, J., Kuzmiak, V., Kwiecien, P., Richter, I.: Silicon waveguides with graphene: Coupling of waveguide mode to surface plasmons. J. Opt. **22**(9), 095801 (2020)

Emani, N.K., Wang, D., Chung, T.-F., et al.: Plasmon resonance in multilayer graphene nanoribbons. Laser & Photonics Reviews **9**(6), 650–655 (2015)

Fei, Z., Andreev, G.O., Bao, W., et al.: Infrared nanoscopy of Dirac plasmons at the graphene-SiO_2 interface. Nano Lett. **11**, 4701–4705 (2011)

Grigorenko, A.N., Polini, M., Novoselov, K.S.: Graphene plasmonics. Nature Photonics **6**, 749–758 (2012)

Hanson, G.W.: Dyadic Green's functions and guided surface waves for a surface conductivity model of graphene. J. Appl. Phys. **103**, 064302 (2008)

Haus, H.A., Huang, W.-P., Kawakami, S., Whitaker, N.A.: Coupled-mode theory of optical waveguides. J. Light. Technol. **5**(1), 16–23 (1987)

Jablan, M., Buljan, H., Soljačič, M.: Plasmonics in graphene at infrared frequencies. Phys. Rev. B - Condens. Matter Mater. Phys. **80**, 245435 (2009)

Jang, M.S., Kim, S., Brar, V.W., Menabde, S.G., Atwater, H.A.: Modulated resonant transmission of graphene plasmons across λ/50 a plasmonic waveguide gap. Phys. Rev. Appl. **10**, 54053 (2018)

Ju, L., Geng, B., Horng, J., et al.: Graphene plasmonics for tunable terahertz metamaterials. Nature Nanotechnology **6**, 630–634 (2011)

Kischkat, J., Peters, S., Gruska, B., et al.: Mid-infrared optical properties of thin films of aluminum oxide, titanium dioxide, silicon dioxide, aluminum nitride, and silicon nitride. Appl. Opt. **51**(28), 6789–6798 (2012)

Koester, S.J., Li, M.: High-speed waveguide-coupled graphene-on-graphene optical modulators. Appl. Phys. Lett. **100**(17), 171107 (2012)

Koester, S.J., Li, M.: Waveguide-coupled graphene optoelectronics. IEEE J. Sel. Top. Quantum Electron. **20**(1), 6000211 (2014)

Kogelnik, H.: Theory of dielectric waveguides. Topics in applied physics. In: Tamir, T. (ed.) Integrated optics, pp. 13–81. Springer, Berlin (1975)

Koppens, F.H.L., Chang, D.E., García De Abajo, F.J.: Graphene plasmonics: A platform for strong light-matter interactions. Nano Lett. **11**(8), 3370–3377 (2011)

Li, W., Chen, B., Meng, C., et al.: Ultrafast all-optical graphene modulator. Nano Lett. **14**, 955–959 (2014)

Liu, M., Yin, X., Ulin-Avila, E., Geng, B., Zentgraf, T., Ju, L., Wang, F., Zhang, X.: A graphene-based broadband optical modulator. Nature **474**, 64–67 (2011)

Mikhailov, S.A., Ziegler, K.: New electromagnetic mode in graphene. Phys. Rev. Lett. **99**, 016803 (2007)

Mohsin, M., Neumaier, D., Schall, D., Otto, M., Matheisen, C., Giesecke, A.L., Sagade, A.A., Kurz, H.: Experimental verification of electro-refractive phase modulation in graphene. Sci. Rep. **5**, 10967 (2015)

Nikitin, A.Y., Guinea, F., García-Vidal, F.J., Martín-Moreno, L.: Edge and waveguide terahertz surface plasmon modes in graphene microribbons. Physical Review B **84**, 161407 (2011)

Nikitin, A.Y., Alonso-Gonzalez, P., Hillenbrand, R.: Efficient Coupling of Light to Graphene Plasmons by Compressing Surface Polaritons with Tapered Bulk Materials. Nano Lett. **14**, 2896–2901 (2014)

Ono, M., Hata, M., Tsunekawa, M., et al.: Ultrafast and energy-efficient all-optical switching with graphene-loaded deep-subwavelength plasmonic waveguides. Nat. Photonics **14**, 37–43 (2020)

Ralevič, U., Isič, G., Vasič, B., Gajič, R.: Modulating light with graphene embedded into an optical waveguide. J. Phys. D Appl. Phys. **47**, 335101 (2014)

Shkondin, E., Takayama, O., Aryaee Panah, M.E., et al.: Large-scale high aspect ratio Al-doped ZnO nanopillars arrays as anisotropic metamaterials. Opt. Mater. Express **7**(5), 1606–1627 (2017)

Sorianello, V., De Angelis, G., Cassese, T.: Complex effective index in graphene-silicon waveguides. Opt. Express **24**(26), 29984 (2016)

Sorianello, V., Midrio, M., Contestabile, G., Asselberghs, I., Van Campenhout, J., Huyghebaert, C., Goykhman, I., Ott, A.K., Ferrari, A.C., Romagnoli, M.: Graphene–silicon phase modulators with gigahertz bandwidth. Nature Photonics **12**, 40–44 (2018)

Sorianello, V., Contestabile, G., Romagnoli, M.: Graphene on Silicon Modulators. J. Light. Technol. **38**(10), 2781–2788 (2020)

Ye, F., Mihalache, D., Hu, B., Panoiu, N.C.: Subwavelength plasmonic lattice solitons in arrays of metallic nanowires. Phys. Rev. Lett. **104**(10), 106802 (2010)

Zhang, Q., Li, X., Hossain, M.M., et al.: Graphene surface plasmons at the near-infrared optical regime. Sci. Rep **4**, 6559 (2014)